

Competing magnetic correlations across the ferromagnetic quantum critical point in the Kondo system $\text{CeTi}_{1-x}\text{V}_x\text{Ge}_3$: ^{51}V NMR as a local probe

M. Majumder^{1,*}, W. Kittler², V. Fritsch^{2,3}, H. v. Löhneysen^{2,4,†}, H. Yasuoka¹ and M. Baenitz^{1,‡}

¹Max Plank Institute for Chemical Physics of Solids, 01187 Dresden, Germany

²Physics Institute, Karlsruhe Institute of Technology, 76131 Karlsruhe, Germany

³Experimental Physics VI, Center for Electronic Correlations and Magnetism, Institute of Physics, University of Augsburg, 86135 Augsburg, Germany

⁴Institute for Solid State Physics, Karlsruhe Institute of Technology, 76012 Karlsruhe, Germany



(Received 6 July 2019; revised manuscript received 7 October 2019; published 25 October 2019)

^{51}V nuclear magnetic resonance (NMR) and magnetization studies on $\text{CeTi}_{1-x}\text{V}_x\text{Ge}_3$ have been performed to explore the evolution from the ferromagnetic ($x = 0.113$) to the antiferromagnetic Kondo lattice state ($x = 1$), with focus on the emergence of a possible ferromagnetic quantum critical point (FMQCP) at $x_c \approx 0.4$. From the temperature dependence of the nuclear spin-lattice relaxation rate, $1/T_1T$, and the Knight shift, K , for $x = 0.113$ and $x = 1$ a considerable competition between ferro- and antiferromagnetic correlations is found. Around the critical concentration ($x = 0.35, 0.405$), quantum-critical spin fluctuations entail weak antiferromagnetic spin fluctuations admixed with ferromagnetic spin fluctuations. The FMQCP in $\text{CeTi}_{1-x}\text{V}_x\text{Ge}_3$ therefore is not purely ferromagnetic in nature.

DOI: [10.1103/PhysRevB.100.134432](https://doi.org/10.1103/PhysRevB.100.134432)

I. INTRODUCTION

The generic Doniach diagram of heavy-fermion materials is based on the competition of Ruderman-Kittel-Kasuya-Yosida (RKKY) interaction between localized magnetic moments, and Kondo interaction between moments and conduction electrons. It has been derived for an antiferromagnetic (AF) and isotropic RKKY type of exchange interaction [1]. For $4f$ systems this competition is a prime scenario for the emergence of a quantum phase transition with a critical point (QCP) at zero temperature. The tuning of AF correlated $4f$ systems by an external control parameter (e.g., chemical composition, hydrostatic or uniaxial pressure, or magnetic field) towards an antiferromagnetic quantum critical point has been demonstrated for many materials [2–4]. The more recent search for ferromagnetic (FM) quantum critical points (FMQCPs) among $4f$ and $3d$ systems [5] has provided a number of examples. However, due to the interplay between FM and AF correlations and, even more importantly, the low-lying quasiparticle excitations in metallic systems, these systems often undergo transitions to other phases and thus appear to “avoid” a bona fide FMQCP. For correlated Yb systems, FM order is rare and so far YbNi_4P_2 is the only FM $4f$ system (with a Curie temperature T_C of 170 mK) which could be tuned towards the FMQCP [6]. Among the Ce systems, CeRuPO [7], CeRu_2Ge_2 [8], CeAgSb_2 [9], and

CeNiSb_2 [10] exhibit FM order but application of hydrostatic pressure induces long-range AF order, thus avoiding an FMQCP. In CeFePO [11] and $\text{CePd}_{1-x}\text{Rh}_x$ [12] a glasslike “Kondo cluster” state forms which likewise impedes tuning towards an FMQCP.

NMR measurements were carried out on a number of those systems to probe locally the magnetic fluctuations and unveil their nature (AF vs FM fluctuations) by temperature and field scaling of the spin-lattice relaxation rate, $1/T_1T$, and the NMR shift, K . In particular, NMR is able to qualitatively disentangle finite- q (AF) and $q = 0$ (FM) excitations [13,14]. At the same time, NMR provides information about the degree of disorder in alloy systems which might affect the nature of the quantum critical point. For example, in the heavy-fermion compound CeFePO where long-range order is absent, ^{31}P NMR gave clear evidence for FM correlations admixed to AF correlations [15], whereas in the structural homolog CeRuPO the existence of stable long-range FM order was demonstrated by ^{31}P NMR measurements [7].

Recently, Kittler *et al.* succeeded in tuning the Curie temperature of the FM Kondo-lattice system CeTiGe_3 ($T_C \approx 14$ K) monotonically down to $T = 0$, indicating a possible FMQCP upon V substitution for Ti [16,17]. T_C decreases linearly with increasing V concentration; the structure type (hexagonal perovskite $P6_3/mmc$; see Fig. 6) is preserved and no crossover to other phases occurs. Upon V substitution the c/a ratio is reduced [16]. The single-ion anisotropy of the Ce^{3+} ions arising from the effect of the crystal electric field (CEF) on the $4f$ moments changes drastically with increasing V content: while the easy direction is parallel to the c axis for CeVGe_3 [17,18]. The end member on the V-rich side, CeVGe_3 , is an antiferromagnetic Kondo system with a Néel temperature T_N of about 6 K and a

*Present address: Experimental Physics VI, Center for Electronic Correlations and Magnetism, University of Augsburg, Germany; mayukh.cu@gmail.com

†Hilbert.loehneysen@kit.edu

‡Michael.Baenitz@cpsf.mpg.de

TABLE I. Summary of estimated parameters of $\text{CeTi}_{1-x}\text{V}_x\text{Ge}_3$.

$\text{CeTi}_{1-x}\text{V}_x\text{Ge}_3$	$x = 0.113$	$x = 0.35$	$x = 0.405$	$x = 1$
T_0 (K)	22.9	21	11	
$1/T_1T$ (1/sK) at 4 K	18.6	50	45	33
A_{hf}^{iso} (T/ μ_B)	0.9	0.6	0.5	1.1
$K(\alpha)$		0.28 ± 0.02	0.46 ± 0.05	

Kondo temperature of $T_K \approx 10$ K [18]. It should be noted that, in contrast to most systems discussed above, the V substitution of Ti in CeTiGe_3 is not isoelectronic but differs by one d electron. Recent studies on CeTiGe_3 suggest an avoided FMQCP and a splitting of the $T_C(p)$ line into a winglike structure [19] as observed in other clean ferromagnets [5], with the complication of several intermediate AF phases occurring in this system.

II. EXPERIMENTAL DETAILS

$\text{CeTi}_{1-x}\text{V}_x\text{Ge}_3$ alloys crystallize in the hexagonal perovskite (BaNiO_3 -type) structure (space group $P6_3/mmc$) without any structural phase transitions across the entire V concentration range. The samples ($x = 0.113, 0.35, 0.405$, and 1) used in this experiment were cut from single crystals [17] and ground to powder. The ^{51}V NMR spectra were taken by the transient (pulsed) NMR technique with a commercial NMR spectrometer (TecMag Apollo). The NMR line profiles were obtained by integration of the spin-echo amplitude in the time domain with sweeping an external field at constant frequency. By simulating the experimental line profile, the isotropic and anisotropic (from the V local symmetry an axial distribution of shift is expected; see Fig. 6) Knight shifts (K_{iso} and K_{ax}) have been extracted. The spin-lattice relaxation rate $1/T_1$ was measured by the saturation recovery method where the recovery of nuclear magnetization was fitted to a stretched exponential function (see Fig. 11).

In general, NMR probes the hyperfine field at the nuclear site originating from the electron magnetic moment which has static and dynamic components. The ^{51}V nucleus (natural abundance 100%) has a nuclear spin of $I = 7/2$; hence a quadrupolar splitting is expected under an electric field gradient (EFG). However, the absence of such satellites indicates a small EFG at the V nuclear site. We have also checked by simulation that even if there is a quadrupolar effect, that is less than 100 kHz, it does not contribute to the temperature dependence of the shift parameters. This is originated by the fact that the ^{51}V nucleus has a small quadrupole moment (0.051 b) and that the EFG usually is screened by conduction electrons in a metal, so the ^{51}V ν_Q effect has been ignored in our study. The temperature-dependent static part of the hyperfine field can be measured by the NMR (Knight) shift, $K(T)$, which is related to the electron spin susceptibility, $\chi(T)$, by $K(T) = (A_{hf}/N\mu_B)\chi(T) + K_0$, where A_{hf} is the hyperfine coupling constant between the nuclear and the electron spins, and K_0 is a temperature-independent contribution. In metals, K_0 arises from both the orbital interaction associated with non- s electrons and the Fermi contact interaction from s conduction electrons ($K_0 = K_{orb} + K_{ce}$). For noncubic materials like $\text{CeTi}_{1-x}\text{V}_x\text{Ge}_3$, the Knight shift is anisotropic,

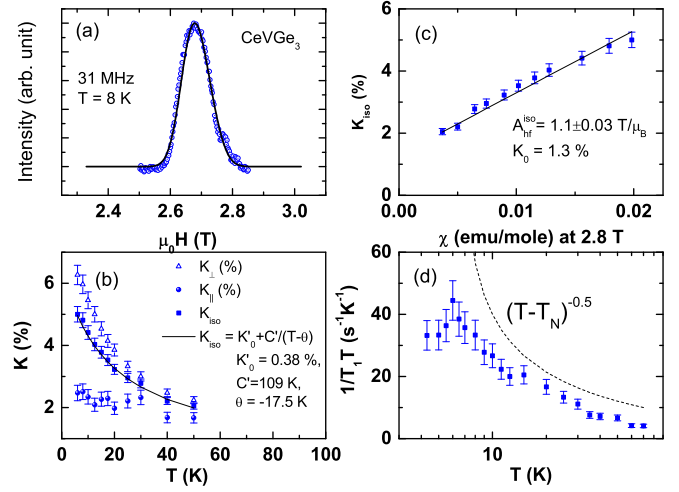


FIG. 1. NMR data for $x = 1$ sample. (a) ^{51}V NMR spectra measured at 31 MHz at 8 K; solid line is a fit of a Gaussian line profile to the data. (b) Temperature dependence of K_{\perp} (open triangles), K_{\parallel} (closed circles), and the resultant K_{iso} ; solid line is a fit of a Curie-Weiss law to the K_{iso} data. (c) K_{iso} vs χ measured at 2.8 T; solid line is a linear fit of the data. (d) Temperature dependence of $1/T_1T$; dashed line is an expected curve of the SCR theory for an itinerant AF magnet.

reflecting the anisotropy of the spin susceptibility. In this case, one observes a powder pattern of the NMR spectrum arising from the different orientation of the crystallites with respect to applied field direction. For the present uniaxial case, we can extract values of K_{\parallel} (B_0 is parallel to the symmetry axis) and K_{\perp} (B_0 perpendicular to the symmetry axis) from the singularities of the spectrum. Then isotropic and axial Knight shifts, K_{iso} and K_{ax} , respectively, are given by

$$K_{iso} = (K_{\parallel} + 2K_{\perp})/3, \quad K_{ax} = (K_{\parallel} - K_{\perp})/3. \quad (1)$$

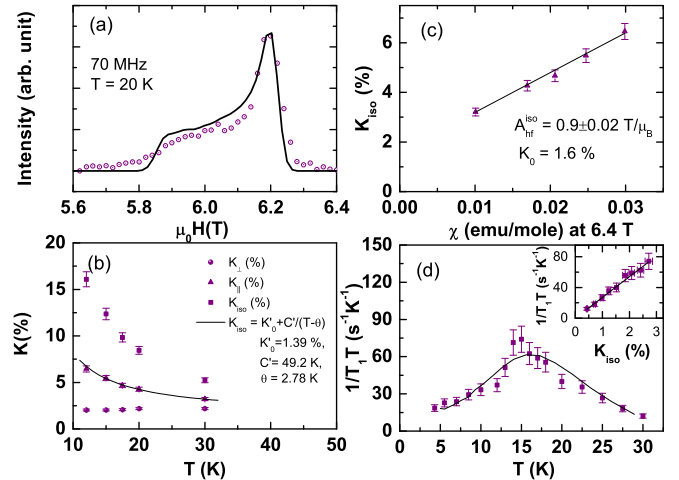


FIG. 2. NMR data for the $x = 0.113$ sample. (a) ^{51}V NMR spectra measured at 70 MHz at 20 K; (b) temperature dependence of K_{\perp} , K_{\parallel} , and the calculated K_{iso} ; (c) K_{iso} (%) vs χ measured at 2.8 T; and (d) temperature dependence of $1/T_1T$. The solid line is a fit of Eq. (3) to the data (for details see main text); the inset shows $1/T_1T$ vs K_{iso} .

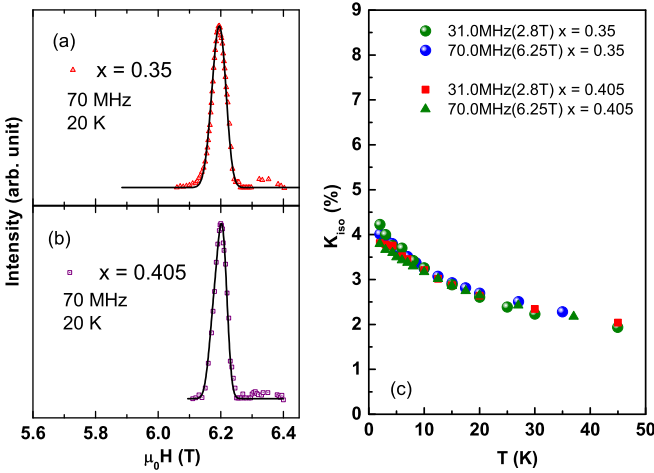


FIG. 3. ^{51}V NMR spectra measured at 70 MHz and 20 K for (a) $x = 0.35$ and (b) 0.405 ; (c) K_{iso} for $x = 0.35$ and 0.405 sample as a function of temperature in two different fields.

Note that in the present case K_{\parallel} corresponds to K parallel to the c axis and K_{\perp} to K perpendicular to the c axis. It is to be noted that we have found a considerable change in the magnitude of A_{hf} with doping (listed in Table I). Such a variation can be due to the change of lattice constant, along with the change of electronic structure (due to electron doping in the present case) as well. Replacing Ti^{4+} by V^{5+} introduces carriers (doping) into the system while the structure type is preserved. It reduces the c/a ratio and changes the single-ion anisotropy of the Ce^{3+} ion. The competition between these two effects might result in the observed considerable change in A_{hf} .

The fluctuating part of the hyperfine field is related to the spin-lattice relaxation rate $1/T_1$, given by

$$1/T_1 \propto T \sum_q |A_{hf}(q)|^2 \chi''_{\perp}(q, \omega_n) / \omega_n. \quad (2)$$

where the sum extends over the wave vectors q within the first Brillouin zone, $\chi''_{\perp}(q, \omega_n)$ is the imaginary part of the transverse dynamical electron spin susceptibility, and ω_n is the Larmor frequency for NMR. $A_{hf}(q)$ is the q -dependent hyperfine coupling constant.

The recovery of the nuclear magnetization, $M(t)$, in these inhomogeneously broadened cases generally follows a stretched exponential form; then the recovery data are fitted to $M(t) = (1 - \exp(-t/T_1)^{\beta})$, where t is the time after a saturation of nuclear magnetization and β is the stretch exponent related to the distribution of the T_1 value across the spectrum.

III. RESULTS AND DISCUSSIONS

Before discussing the compounds close to the FMQCP ($x = 0.35$ and 0.405), we present the results for the parent compounds (AF, $x = 1.0$, and FM, $x = 0.113$).

CeVGe_3 ($x = 1$) is a heavy-fermion itinerant antiferromagnet with $T_K \approx 10$ K and $T_N \approx 6$ K. The ^{51}V NMR spectra have been taken at a fixed frequency of 31.0 MHz. The field-swept ^{51}V NMR spectra at 8 K, the temperature dependence of K_{iso} , and the relaxation rate divided by temperature, $1/T_1 T$, are

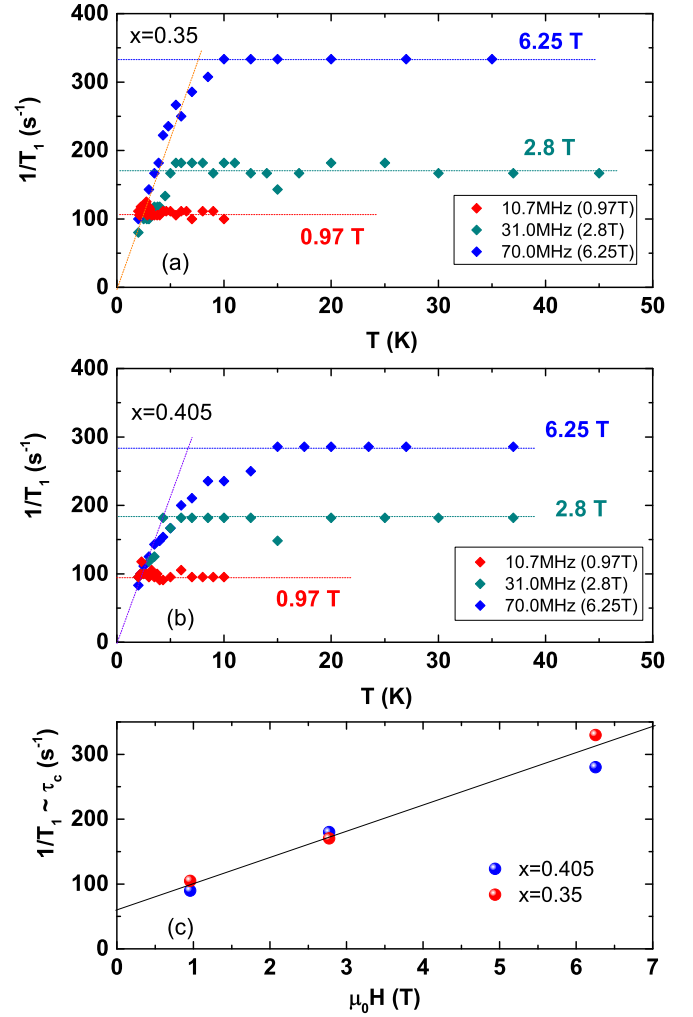


FIG. 4. $1/T_1$ vs temperature T for (a) $x = 0.35$ and (b) $x = 0.405$ at different fields (c) τ_c (correlation time of the spin fluctuations) as a function of applied field. The dotted and solid lines are to guide the eye.

depicted in Figs. 1(a), 1(b), and 1(d), respectively. In order to obtain the isotropic hyperfine coupling constant A_{hf}^{iso} , the observed K_{iso} data are plotted as a function of the magnetic susceptibility (χ) with the temperature as an implicit parameter in Fig. 1(c). From the slope and the intercept, A_{hf}^{iso} and K_{orb} are obtained as 1.1 T/Ce- μ_B and 1.3%, respectively. Here, A_{hf}^{iso} indicates that if a Ce $4f$ moment is polarized by $1\mu_B$, the V nucleus is subjected to an isotropic hyperfine field of 1.1 T along the field direction.

K_{iso} , and hence the static susceptibility χ , has a strong temperature dependence, implying that the wave-vector-dependent susceptibility $\chi(q)$ has not only a peak at wave vector $q = Q$ but also must have a large FM $q = 0$ component. As to the $1/T_1 T$ vs T plot in Fig. 1(d), the self-consistent renormalization (SCR) theory for a weak itinerant AF predicts a $1/T_1 T \propto 1/\sqrt{T - T_N}$ divergence at T_N [20]. Although there is an anomaly at T_N in $1/T_1 T$, the experimental data cannot be described by the above relation. This is also an evidence for the existence of FM fluctuations, which is suppressed by an external field around T_N .

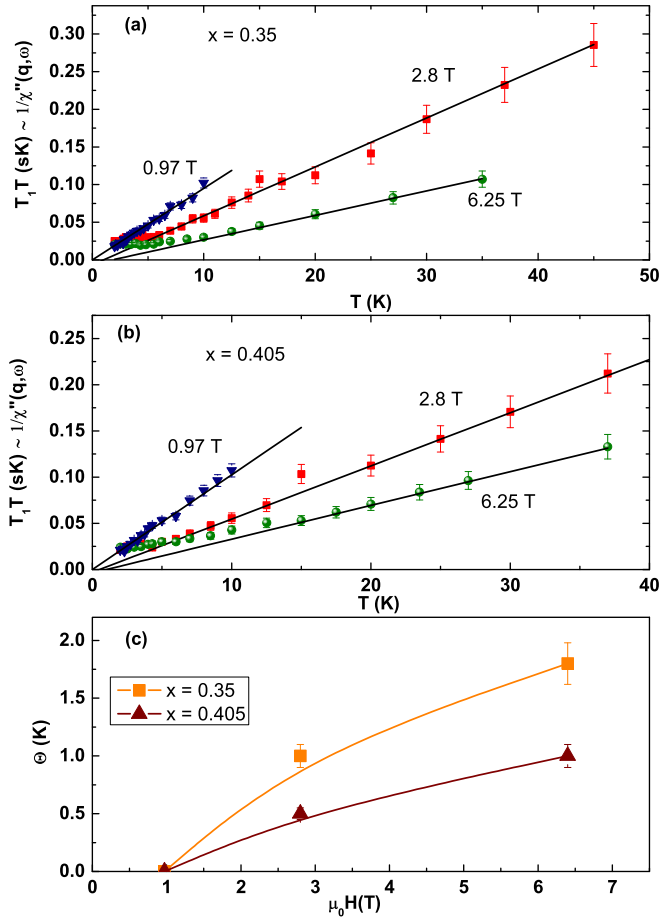


FIG. 5. Temperature dependence of $1/T_1T$ at different fields for (a) $x = 0.35$ and (b) $x = 0.405$. (c): θ obtained from high-temperature Curie-Weiss fits (straight lines) as a function of field for $x = 0.35$ and 0.405 . The curved lines are to guide the eye.

For the other end member of the series we have taken the $x = 0.113$ sample which undergoes FM ordering at $T_C \approx 9$ K in zero field (as determined from the sharp maximum in the specific heat [17]). The ^{51}V NMR spectrum shown in Fig. 2(a) exhibits a large anisotropy ($K_{\perp}/K_{\parallel} \approx 0.26$ at 20 K), which is consistent with the anisotropy in the magnetic susceptibility reported for single crystals [17,21]. As described below, the anisotropy tends to vanish towards the FMQCP but increases again in CeVGe_3 where the anisotropy is reversed to yield $K_{\perp}/K_{\parallel} \approx 2.37$ at 8 K, again in accord with the susceptibility measurements [16,17].

The temperature dependence of K_{iso} extracted from K_{\parallel} and K_{\perp} is shown in Fig. 2(b), and that of $1/T_1T$ in Fig. 2(d). Although $1/T_1T$ scales with K_{iso}^2 (Korringa law) in simple metals, $1/T_1T$ for $x = 0.113$ depends linearly on K_{iso} as shown in the inset of Fig. 2(d). This behavior can be described by SCR theory for a weak itinerant ferromagnet in the frame of SCR theory. In SCR theory, $1/T_1T$ under an external field is given by [20,22,23]

$$(1/T_1T) = \kappa \chi / (1 + \chi^3 B_0^2 P), \quad (3)$$

which reproduces very well the experimental $1/T_1T(T)$ shown in Fig. 2(d) for $B_0 = 6.25$ T. Here, P is a constant related

to the area of the Fermi surface of the itinerant electrons, and κ is related to the spin-fluctuation parameter, T_0 . In the paramagnetic state

$$1/T_1T \approx 3\hbar\gamma_n^2 A_{hf} K_{\text{iso}} / 16\pi \mu_B T_0. \quad (4)$$

The slope of $1/T_1T$ vs K_{iso} in the inset of Fig. 2(d) yields the value $T_0 = 21$ K, which is rather close to T_C . The deviation from 1 of the ratio T_C/T_0 is a measure of the degree of itinerancy of the $4f$ electrons [20,22–24]. $T_C \approx T_0$ indicates that the enhancement of $\chi(q)$ is not confined to $q = 0$ but rather extends to larger q values. This situation is reminiscent of but opposite that of $x = 1$ described above, where $\chi(q)$ extends from the AF wave vector Q towards $q = 0$. Therefore, we conclude that there is a considerable mixture of FM and AF correlations in both end materials.

We now discuss ^{51}V NMR data for the samples with $x = 0.35$ and 0.405 which are close to the proposed FMQCP. Here the NMR measurements were performed under different applied magnetic fields to elucidate the properties in low fields. The spectra shown in Figs. 3(a) and 3(b) for $x = 0.35$ and $x = 0.405$ are less anisotropic compared to those for $x = 1.0$ and 0.113 . The temperature dependence of K_{iso} at 2.76 and 6.25 T is shown in Fig. 3(c). The temperature dependencies of the relaxation rate $1/T_1$ in different fields are shown in Figs. 4(a) and 4(b) for $x = 0.35$ and $x = 0.405$, respectively. $1/T_1$ shows a crossover from a low-temperature Korringa-like process ($1/T_1 \propto T$) to a temperature-independent process above a temperature T^* , which depends on field. SCR theory has been successfully adopted to understand thermodynamic properties of weakly or nearly itinerant FM and AF systems. This model has been extended to cover cases where the spin fluctuations have large amplitudes and their significant q components extend over the entire q space of the first Brillouin zone. This extension of the SCR theory, the “temperature-induced-local-moment” (TILM) model, predicts that the amplitude of local spin fluctuations, $\langle S_L^2 \rangle$, increases rapidly at low temperatures and saturates at a certain temperature T^* [25]. Above T^* , the thermodynamic properties are governed by the transverse component (local-moment type) of the fluctuations and the susceptibility shows Curie-Weiss behavior. As described above, the $1/T_1$ data of $\text{CeTi}_{1-x}\text{V}_x\text{Ge}_3$ around $x \approx 0.4$ are in accord with the TILM model. It has been shown that exchange-coupled local-moment fluctuations bring about a temperature-independent $1/T_1$, a magnitude given by the correlation time τ_c associated with the local spin fluctuations [26]:

$$(1/T_1)_{\text{TILM}} = (A_{hf}/\hbar)^2 \frac{(2\pi)^{1/2} \langle S_L^2 \rangle}{3} \tau_c, \quad (5)$$

where $(1/T_1)_{\text{TILM}}$ is the temperature-independent value observed above T^* , and $\langle S_L^2 \rangle$ is the amplitude of the local spin density. Using experimental values of $(1/T_1)_{\text{TILM}}$ and effective moments (obtained from the Curie-Weiss fit) assumed to be the same as $\langle S_L^2 \rangle$, τ_c is evaluated and shown in Fig. 4(c) as a function of magnetic field. τ_c for both samples around the FMQCP ($x = 0.35$ and 0.405) increases linearly with

field, indicating that the characteristic frequency of the spin fluctuations decreases with external field; i.e., the samples approach the field-polarized state.

A possible microscopic reason for a constant $1/T_1$ value may be the suppression of Kondo interaction with increasing temperature, with a crossover from a T-linear Fermi-liquid-like relaxation rate. Because T_K is around 10 K in $\text{CeTi}_{1-x}\text{V}_x\text{Ge}_3$, the high-temperature relaxation process may be due to fluctuations of purely local moments associated with the thermal quenching of the Kondo interaction. The relaxation rate of this type of process can easily be calculated using the hyperfine coupling constant and an exchange frequency estimated from the Weiss constant [22]. The calculated $1/T_1$ is around $2 \times 10^3 \text{ s}^{-1}$, which is about one order of magnitude larger than the experimental values. Also, if we assume observed T^* is associated with T_K one would expect that the T^* should be decreased with increasing field, which is opposite to the experimental findings. Therefore, we believe TILM is a more plausible scenario to explain the experimental results for the samples close to the quantum critical point.

For a detailed discussion, we plot $T_1 T$ which is a measure of the inverse $\chi''(q, \omega_n)$ [cf. Eq. (2)] as a function of temperature in Figs. 5(a) and 5(b) for $x = 0.35$ and $x = 0.405$. For both samples $1/T_1 T$ above T^* follows the Curie-Weiss (CW) law with the Weiss constant θ increasing with applied magnetic field [Fig. 5(c)]. The enhancement of θ simply illustrates the tendency to a saturated paramagnet with increasing field. The fact that θ for the lowest field for both samples is very close to zero signals quantum critical spin fluctuations. Note that the field-dependent Curie constants correspond to the inverse of τ_c [cf. Eq. (5)].

As shown in Figs. 4(a) and 4(b), at temperatures well below T^* the nuclear relaxation is governed by the Korringa process, where interacting electron-hole excitations are the primary source of the magnetic excitations. Treating the interaction of the quasiparticles in the frame of the random phase approximation (RPA), the modified Korringa relation can be expressed as $S_0/T_1 T K_{\text{spin}}^2 = K(\alpha)$, with $S_0 = (\hbar/4\pi k_B)(\gamma_e/\gamma_n)^2$. $K(\alpha) = \langle (1 - \alpha_0)^2 / (1 - \alpha_q)^2 \rangle_{FS}$ with $\alpha_q = \alpha_0[\chi_0(0, q)/\chi_0(0, 0)]$, where $\chi_0(\omega, q)$ is the magnetic susceptibility, and $\langle \dots \rangle_{FS}$ indicates the q average over the Fermi surface. $K(\alpha)$ is a modification factor of the Korringa relation, which depends on the exchange enhancement factor α . If the spin fluctuations are enhanced around $q = 0$ as for dominant FM correlations, then $K(\alpha) < 1$. On the other hand, $K(\alpha) > 1$ indicates that finite- q (typically AF) spin fluctuations are dominant. The estimated $K(\alpha)$ values for $x = 0.35$ and 0.405 at 2 K (a temperature where the modified Korringa law is valid) are shown in Table I, which indicates that the dominant ferromagnetic correlations are reduced with increasing x or AF correlations are becoming dominant with increasing x towards CeVGe_3 . The change of characteristics in the spin fluctuations can easily be seen from Fig. 12, where $1/T_1 T$ is plotted as a function of temperature for all the different doping concentrations.

Evidence for the presence of weak AF spin fluctuations on top of dominant FM spin fluctuations close to an FMQCP was seen recently in Ru-doped CeFePO [28]. The appearance of AF spin fluctuations was attributed to the Fermi-surface

instability which might appear in the case of a local QCP. The presence of considerable AF correlations for $x = 0.113$ even far away from the possible QCP indicates that the QCP in this system is not driven solely by FM fluctuations. Furthermore, the Knight-shift anisotropy reduces considerably in $\text{CeTi}_{1-x}\text{V}_x\text{Ge}_3$ upon approaching QCP, which indicates the isotropic nature of local fields at the V site. This behavior is very different from that of the layered FM CeRuPO , which is driven to a QCP by substitution of Ru by Fe, where the fluctuations become strongly anisotropic upon approaching the QCP [27,28].

On more general grounds, the issue of an FMQCP remains very challenging despite the considerable amount of work in this field [5]. It is generally believed that a QCP in clean systems is intrinsically unstable because of the dynamics of low-lying fermionic excitations. Therefore, alloy systems with varying degrees of disorder are an important subject. The system $\text{CeTi}_{1-x}\text{V}_x\text{Ge}_3$ is unique in that FM for $x = 0$ gives way to AF for $x = 1$ and, at the same time, the single-ion anisotropy changes from uniaxial (Ising) to planar (XY). Close to the QCP, the system becomes isotropic. It should be mentioned that unusually slowly fluctuating glasslike electronic phases near FM quantum criticality due to the competing interactions have been proposed by theory [29]. In our case, the competition between dominant FM and weak AF correlations might induce such phases which prevents the formation of a pure FMQCP. However, our NMR data do not indicate pronounced line broadening which would signify a glasslike inhomogeneous state. Numerous experiments on clean three-dimensional FM metals have shown that, in contrast to the original Hertz-Millis-Moriya model of quantum criticality, the FMQCP is unstable, and FM metals undergo a first-order phase transition to the paramagnetic or to an incommensurate phase as predicted by theory [30–32]. As a matter of fact, pure CeTiGe_3 under high hydrostatic pressure follows this scenario, with several intervening magnetic phases until the paramagnetic state is finally reached around 6 GPa. Under magnetic field a winglike structure appears at high pressures, again as predicted by theory [33] and observed in other clean systems [34]. For an alloyed system as studied in the present work, with a considerable degree of disorder at the QCP at $x \approx 0.4$, one might expect a genuine second-order transition. Indeed, it was suggested on theoretical grounds that a first-order FM transition might be “tuned” continuously to an FMQCP by disorder [35]. Further work is necessary to elucidate how these features compete or cooperate at the QCP. In this respect it is worth mentioning that our study indicates the presence of anisotropy in shift, which in principle should also induce anisotropy in the relaxation processes. The effects of anisotropy in general have not been included in our present study, especially in the case of interpreting the nature of spin fluctuations as it is not possible to estimate the relaxation in different directions without having single crystals. So we have mainly used the isotropic part of the Knight shift and the “average” T_1 by using the stretched exponential function which includes the distribution of T_1 due to the anisotropy and also disorder. The issues related to such anisotropy will be of interest for future studies by employing single crystals.

IV. CONCLUSION

Systematic ^{51}V NMR measurements were performed on $\text{CeTi}_{1-x}\text{V}_x\text{Ge}_3$ with the end members showing ferromagnetic and antiferromagnetic order, for $x = 0$ and $x = 1$, respectively. NMR as a local probe provides information about magnetic fluctuations across the phase diagram. The temperature dependence of K and $1/T_1T$ in CeVGe_3 shows a strong admixture of FM fluctuations to the dominant AF fluctuations. The temperature dependence of $1/T_1T$ for $x = 0.113$ at 6.4 T can be well explained by self-consistent renormalization theory for itinerant ferromagnets. Around the critical concentration ($x = 0.35, 0.405$), quantum-critical spin fluctuations comprise weak but finite AF spin fluctuations admixed to FM spin fluctuations. The spin-fluctuation parameters T_0 and $K(\alpha)$ (the latter probing the relative strength of AF vs FM spin fluctuations) were estimated for $x = 0.35$ and 0.405. $K(\alpha)$ shows a considerable enhancement with x indicating the growing importance of AF fluctuations towards the QCP. The critical samples lack the NMR fingerprint of a pure FMQCP, i.e., the $1/T_1T \sim T^{-4/3}$ NMR power law [36]. Hence, the general presence of both FM and AF fluctuations across the whole $\text{CeTi}_{1-x}\text{V}_x\text{Ge}_3$ is a constituting trait of this system. Further work should elucidate if and how the changing single-ion anisotropies affect the quantum criticality in this system.

ACKNOWLEDGMENTS

We thank M. Brando, C. Geibel, and B. Pilawa for fruitful discussions. Furthermore, we thank H. Rave, C. Klausnitzer, and R. Hempel-Weber for technical support.

APPENDIX A: CRYSTAL STRUCTURE

The crystal structure of $\text{Ce}(\text{V}, \text{Ti})\text{Ge}_3$ is shown in Fig. 6. It crystallizes in the hexagonal perovskite (BaNiO_3 -type) structure $P63/mmc$ with $a = b = 6.306$ (6.2744) Å, $c = 5.6732$ (5.882) Å, $\alpha = \beta = 90^\circ$, and $\gamma = 120^\circ$ for CeVGe_3 (CeTiGe_3). The crystal structure has only one crystallographic V (Ti), Ce, and Ge sites. Figure 6(a) is the full view and Fig. 6(b) is the view along the c axis, showing a uniaxial symmetry of the V-site transferred hyperfine interaction from the Ce sites.

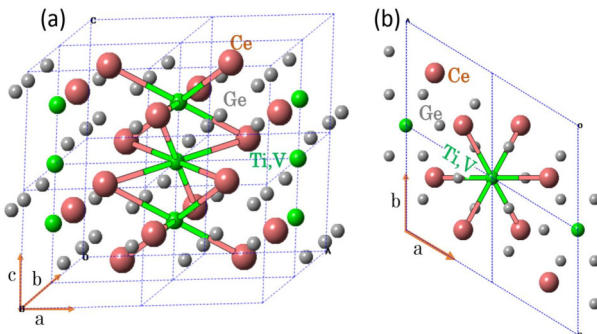


FIG. 6. Crystal structure of $\text{Ce}(\text{Ti}, \text{V})\text{Ge}_3$.

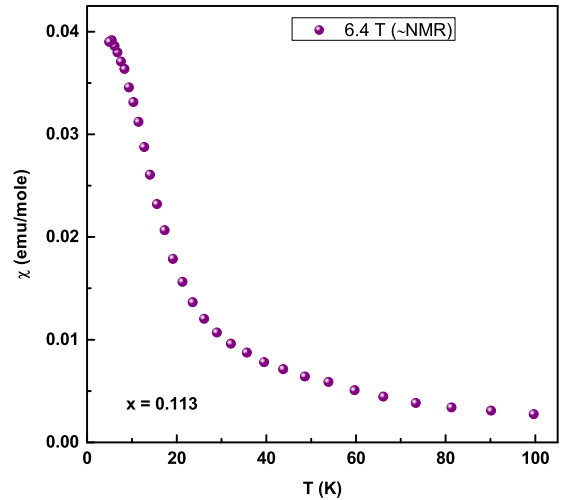


FIG. 7. Temperature dependence of M/H at $\mu_0H = 6.4$ T for the $x = 0.113$ sample.

APPENDIX B: MAGNETIZATION

The dc magnetization was measured in various magnetic fields and temperatures between 5 and 100 K using a commercially available superconducting quantum interference device magnetometer (Quantum Design magnetic property measurement system).

Figure 7 shows the temperature dependence of ($\chi = M/H$) for an $x = 0.113$ sample at 6.4 T, close to which the ^{51}V NMR has been conducted.

Figure 8 also shows the temperature dependence of M/H and $\chi_{ac}(=\delta M/\delta H)$ at different magnetic fields in a log-log plot. We could not find any signature of long-range magnetic ordering. With increasing field the critical behavior of χ has been suppressed for the two samples close to the quantum-critical V concentration, which is also consistent with the results of ^{51}V NMR described in the main text.

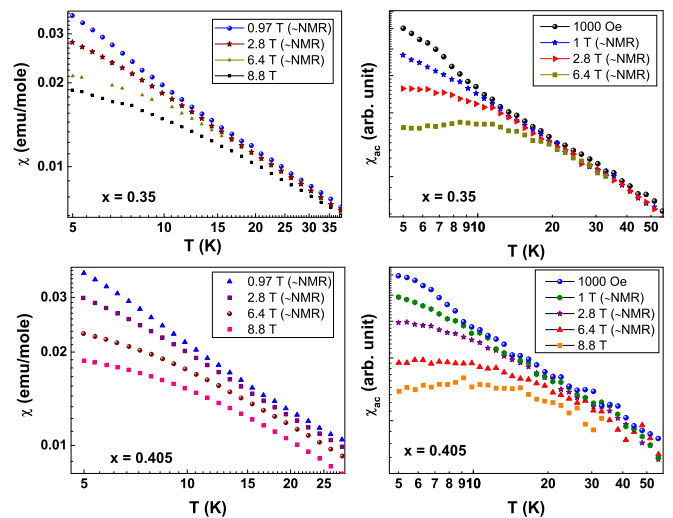


FIG. 8. Temperature dependence of M/H and $\chi_{ac}(=\delta M/\delta H)$ in different magnetic fields (mostly at which ^{51}V has been conducted) for the $x = 0.35$ and 0.405 samples. The fields where ^{51}V NMR was performed are indicated.

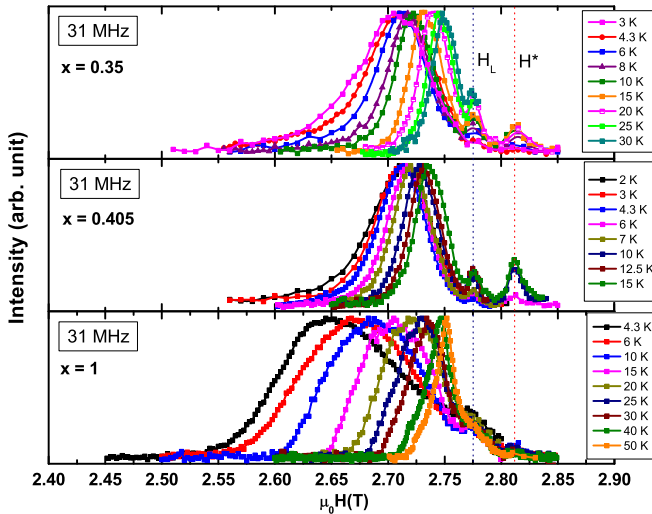


FIG. 9. Field-sweep ^{51}V spectra at 31 MHz. Vertical dotted lines at H_L and H^* (see text) are attributed to nonmagnetic impurity phases.

APPENDIX C: NMR

The ^{51}V NMR spectra were obtained using a commercially available Tecmag NMR spectrometer in the field-sweep mode down to 1.8 K at various resonance frequencies (Fig. 9). NMR measurements were performed on the ^{51}V nucleus with a spin ($I = 7/2$) with 99.75% natural abundance.

The crystal structure of $\text{Ce}(\text{Ti}, \text{V})\text{Ge}_3$ exhibits one V-lattice site. The ^{51}V NMR spectra shows only a single NMR line. There are no further lines (satellites) related to quadrupolar interaction. The spin-echo intensity was obtained by integrating over the spin echo in the time domain at a given magnetic field. The final spectrum is given by plotting the spin-echo intensity as a function of the applied field. Due to the small quadrupolar moment and also small EFG at the V site the satellites are not visible, or they are superimposed with the broadened central line. The spectra for the $x = 0.35$ and 0.405 samples are quite isotropic in nature, whereas for $x = 0.113$,

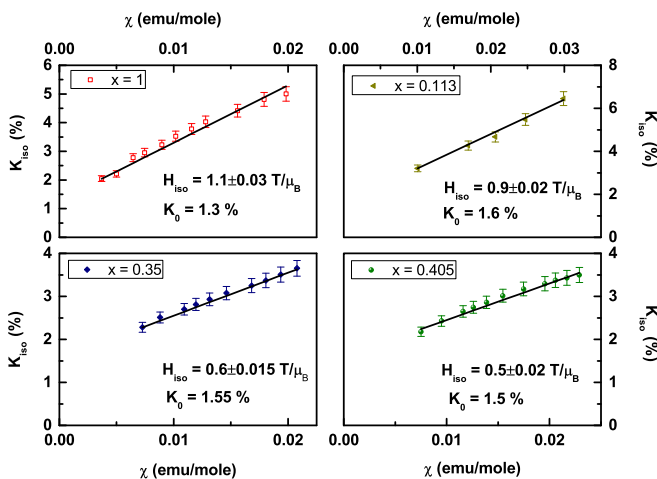


FIG. 10. K_{iso} vs χ for all the samples indicating a linear relation.

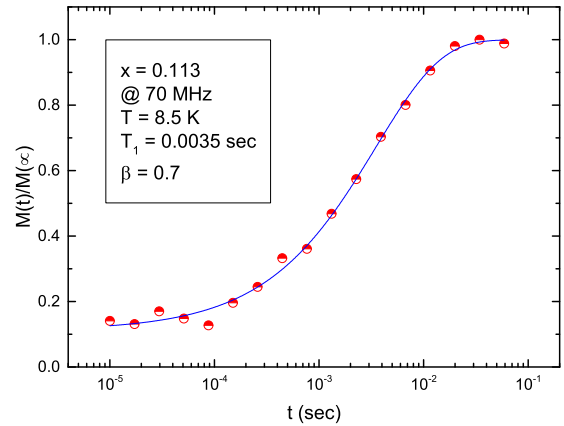


FIG. 11. Magnetization recovery curve at 70 MHz and at 8.5 K for the $x = 0.113$ sample.

the spectra are axially symmetric and for $x = 1$ exhibit planar anisotropy. Interestingly the nature of anisotropy is opposite for both samples ($x = 0.113$ and 1), which we suggest is due to the opposite nature of anisotropy seen from magnetization measurements in single crystals [21]. In addition, we found two extra peaks in almost all spectra. One peak is at the ^{51}V Larmor field (H_L) which indicates the presence of unreacted V_2O_5 . Another peak (at H^*) has a negative (but also temperature-independent) shift which might originate from a binary V^{5+} -containing phase (probably a V-Ge binary phase).

To estimate the hyperfine coupling constants A_{hf}^{iso} , $K_{\text{iso}}(\%)$ is plotted vs χ (Fig. 10) and found to follow a linear relation as expected. From the slope we estimate A_{hf}^{iso} , which is plotted in Fig. 4 in the main text for all samples investigated.

The spin-lattice relaxation rate was obtained by the standard saturation-recovery method. The exponent $\beta \approx 0.7-0.75$ was kept constant for all temperatures for $x = 0.35, 0.405$, and 0.113 but $\beta = 1$ for the pure end member with $x = 1$. A typical recovery curve is shown in Fig. 11.

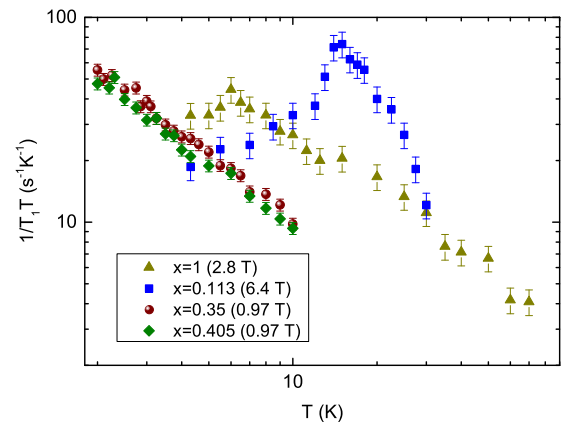


FIG. 12. Temperature dependence of $1/T_1 T$ at the respective lowest fields for each of the compounds. The figure indicates the doping evolution of electron spin dynamics in $\text{CeTi}_{1-x}\text{V}_x\text{Ge}_3$.

- [1] S. Doniach, in *Valence Instabilities and Related Narrow Band Phenomena*, edited by R. D. Parks (Plenum, New York, 1977), p. 1669.
- [2] H. V. Löhneysen, A. Rosch, M. Vojta, and P. Wolfle, *Rev. Mod. Phys.* **79**, 1015 (2007).
- [3] P. Gegenwart, Q. Si, and F. Steglich, *Nat. Phys.* **4**, 186 (2008).
- [4] Q. Si and F. Steglich, *Science* **329**, 1161 (2010).
- [5] M. Brando, D. Belitz, F. M. Grosche, and T. R. Kirkpatrick, *Rev. Mod. Phys.* **88**, 025006 (2016).
- [6] A. Steppke, R. Kuchler, S. Lausberg, E. Lengyel, L. Steinke, R. Borth, T. Lühmann, C. Krellner, M. Nicklas, C. Geibel *et al.*, *Science* **339**, 933 (2013).
- [7] C. Krellner, N. S. Kini, E. M. Brüning, K. Koch, H. Rosner, M. Nicklas, M. Baenitz, and C. Geibel, *Phys. Rev. B* **76**, 104418 (2007).
- [8] S. Süllow, M. C. Aronson, B. D. Rainford, and P. Haen, *Phys. Rev. Lett.* **82**, 2963 (1999).
- [9] V. A. Sidorov, E. D. Bauer, N. A. Frederick, J. R. Jeffries, S. Nakatsuji, N. O. Moreno, J. D. Thompson, M. B. Maple, and Z. Fisk, *Phys. Rev. B* **67**, 224419 (2003).
- [10] V. A. Sidorov, E. D. Bauer, H. Lee, S. Nakatsuji, J. D. Thompson, and Z. Fisk, *Phys. Rev. B* **71**, 094422 (2005).
- [11] S. Lausberg, J. Spehling, A. Steppke, A. Jesche, H. Luetkens, A. Amato, C. Baines, C. Krellner, M. Brando, C. Geibel, H.-H. Klauss, and F. Steglich, *Phys. Rev. Lett.* **109**, 216402 (2012).
- [12] T. Westerkamp, M. Deppe, R. Kuchler, M. Brando, C. Geibel, P. Gegenwart, A. P. Pikul, and F. Steglich, *Phys. Rev. Lett.* **102**, 206404 (2009).
- [13] M. Baenitz, R. Sarkar, P. Khuntia, C. Krellner, C. Geibel, and F. Steglich, *Phys. Status Solidi C* **3**, 540 (2013).
- [14] R. Sarkar, P. Khuntia, C. Krellner, C. Geibel, F. Steglich, and M. Baenitz, *Phys. Rev. B* **85**, 140409(R) (2012).
- [15] E. M. Bruning, C. Krellner, M. Baenitz, A. Jesche, F. Steglich, and C. Geibel, *Phys. Rev. Lett.* **101**, 117206 (2008).
- [16] W. Kittler, V. Fritsch, F. Weber, G. Fischer, D. Lamago, G. Andre, and H. v. Löhneysen, *Phys. Rev. B* **88**, 165123 (2013).
- [17] W. Kittler, Ph.D. thesis, Karlsruhe Institute of Technology, 2014, <https://www.ksp.kit.edu/download/1000046409>.
- [18] W. Kittler, V. Fritsch, B. Pilawa, M. Baenitz, P. C. Canfield, and H. V. Löhneysen (unpublished).
- [19] U. S. Kaluarachchi, V. Taufour, S. L. Budko, and P. C. Canfield, *Phys. Rev. B* **97**, 045139 (2018).
- [20] T. Moriya, *Spin Fluctuations in Itinerant Electron Magnetism* (Springer-Verlag, New York, 1985).
- [21] M. Inamdar, A. Thamizhavel, and S. K. Dhar, *J. Phys.: Condens. Matter* **26**, 326003 (2014).
- [22] T. Moriya, *Prog. Theor. Phys.* **16**, 23 (1956).
- [23] T. Moriya, *J. Phys. Soc. Jpn.* **18**, 516 (1963).
- [24] M. Majumder, K. Ghoshray, A. Ghoshray, B. Bandyopadhyay, and M. Ghosh, *Phys. Rev. B* **82**, 054422 (2010).
- [25] T. Moriya, *Solid State Commun.* **26**, 483 (1978).
- [26] N. Inoue and H. Yasuoka, *Solid State Commun.* **30**, 341 (1979).
- [27] S. Kitagawa, K. Ishida, T. Nakamura, M. Matoba, and Y. Kamihara, *J. Phys. Soc. Jpn.* **82**, 033704 (2013).
- [28] S. Kitagawa, K. Ishida, T. Nakamura, M. Matoba, and Y. Kamihara, *Phys. Rev. Lett.* **109**, 227004 (2012).
- [29] Z. Nussinov, I. Vekhter, and A. V. Balatsky, *Phys. Rev. B* **79**, 165122 (2009).
- [30] A. V. Chubukov, C. Pepin, and J. Rech, *Phys. Rev. Lett.* **92**, 147003 (2004).
- [31] D. Belitz and T. R. Kirkpatrick, *Rev. Mod. Phys.* **66**, 261 (1994).
- [32] D. Belitz and T. R. Kirkpatrick, *Phys. Rev. B* **56**, 6513 (1997).
- [33] D. Belitz, T. R. Kirkpatrick, and J. Rollbühler, *Phys. Rev. Lett.* **94**, 247205 (2005).
- [34] V. Taufour, U. S. Kaluarachchi, R. Khasanov, M. C. Nguyen, Z. Guguchia, P. K. Biswas, P. Bonfa, R. De Renzi, X. Lin, S. K. Kim, E. D. Mun, H. Kim, Y. Furukawa, C.-Z. Wang, K.-M. Ho, S. L. Bud'ko, and P. C. Canfield, *Phys. Rev. Lett.* **117**, 037207 (2016).
- [35] Y. Sang, D. Belitz, and T. R. Kirkpatrick, *Phys. Rev. Lett.* **113**, 207201 (2014).
- [36] M. Majumder, M. Wagner-Reetz, R. Cardoso-Gil, P. Gille, F. Steglich, Y. Grin, and M. Baenitz, *Phys. Rev. B* **93**, 064410 (2016).